ACS APPLIED MATERIALS & INTERFACES

Research Article

Cite This: ACS Appl. Mater. Interfaces XXXX, XXX, XXX−XXX

www.acsami.org

Chemical Doping Effects in Multilayer MoS_2 and Its Application in Complementary Inverter

Hocheon Yoo,[†] Seongin Hong,[§] Sungmin On,[†] Hyungju Ahn,[‡] Han-Koo Lee,[‡] Young Ki Hong,[§] Sunkook Kim,*[,§] and Jae-Joon Kim*[,†]

[†]Department of Creative IT Engineering and [‡]Pohang Accelerator Laboratory, Pohang University of Science and Technology, Pohang 790-784, Republic of Korea

[§]Multi-Functional Nano/Bio Electronics Laboratory, Sungkyunkwan University, Suwon 440-746, Republic of Korea

Supporting Information

ABSTRACT: Multilayer MoS_2 has been gaining interest as a new semiconducting material for flexible displays, memory devices, chemical/biosensors, and photodetectors. However, conventional multilayer MoS_2 devices have exhibited limited performances due to the Schottky barrier and defects. Here, we demonstrate poly(diketopyrrolopyrrole-terthiophene) (PDPP3T) doping effects in multilayer MoS_2, which results in improved electrical characteristics (~4.6× higher on-current compared to the baseline and a high current on/off ratio of 10^6). Synchrotron-based study using X-ray photoelectron spectroscopy and grazing incidence wide-angle X-ray diffraction provides mechanisms that align the edge-on crystallites (97.5%) of the PDPP3T as well as a larger interaction with MoS_2 that leads to dipole and charge transfer effects (at annealing temperature of 300 °C), which support the observed enhancement of the electrical characteristics. Furthermore, we demonstrate a complementary metal−oxide−semiconductor inverter that uses a p-type $MoSe_2$ and a PDPP3T-doped MoS_2 as charging and discharging channels, respectively.

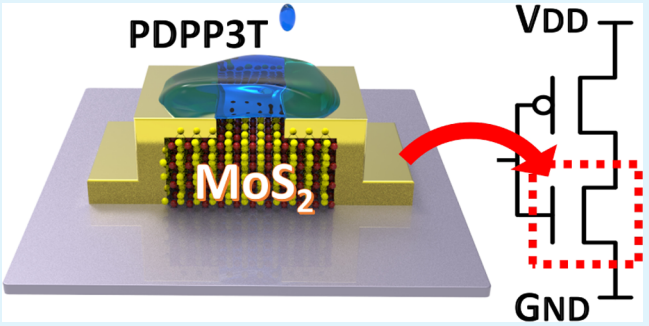

KEYWORDS: *transition-metal dichalcogenides, thin-film transistor, chemical doping, multilayer MoS_2, complementary inverter*

INTRODUCTION

Layered transition-metal dichalcogenides (TMDs) have received scientific interest as new semiconducting materials due to their outstanding properties, such as high carrier mobility,[1,2] low subthreshold swing,[3] and high degree of mechanical flexibility.[4] These high-performance features promise a variety of applications,[5−8] including integrated circuits, flexible displays, memory devices, chemical/biosensors, and photodetectors. In recent years, several groups have demonstrated the high performance of field-effect transistors[9,10] and circuits[5,11] using monolayer and bilayer TMDs, such as molybdenum disulfide (MoS_2) or molybdenum diselenide ($MoSe_2$).

However, even though these TMD electronic devices are perceived to be promising candidates for future semiconductor devices, conventional TMD devices suffer from complex processes that require precise control of monolayers (a single or <3 L), full coverage in large area, and crystal defects. In this regard, multilayer TMDs[12−14] can be an attractive alternative for abovementioned issues due to the relatively simple fabrication as well as more potential advantages, such as higher density of states,[12] more conducting channel in long channel transistors, and a wider spectral response.[15] High electrical performances of multilayer TMD transistors with single-gate dielectric have already been demonstrated, such as a high electron mobility of ~120 $cm^2\ V^{-1}\ s^{-1}$ and a low subthreshold swing of 60 mV dec^{-1}. Therefore, multilayer TMDs have great potential for the fabrication of large area as well as a simple path to commercial process for the aforementioned applications.

However, most of the previous multilayer TMDs suffer from a large contact resistance at the interface between the TMDs and metal electrode due to the Schottky barrier (SB) as well as nonuniform defects.[13,16] These SBs and defects result in lower charge injection, which significantly degrade device performance. Thus, there is a need to devise a solution that compensates for these defects and the SB to improve the electrical properties of multilayer TMDs.

Previous work reported a doping technique on TMDs using organic materials.[16−19] However, all these previous studies have been limited to a target of only single- or few-layer (<5 L) structures of TMDs. Fabrication of these ultrathin TMDs is not simple owing to the complicated process requiring accurate control over the number of layers. In contrast, multilayer

Received: May 29, 2018
Accepted: June 19, 2018
Published: June 19, 2018

DOI: 10.1021/acsami.8b08773
ACS Appl. Mater. Interfaces XXXX, XXX, XXX−XXX

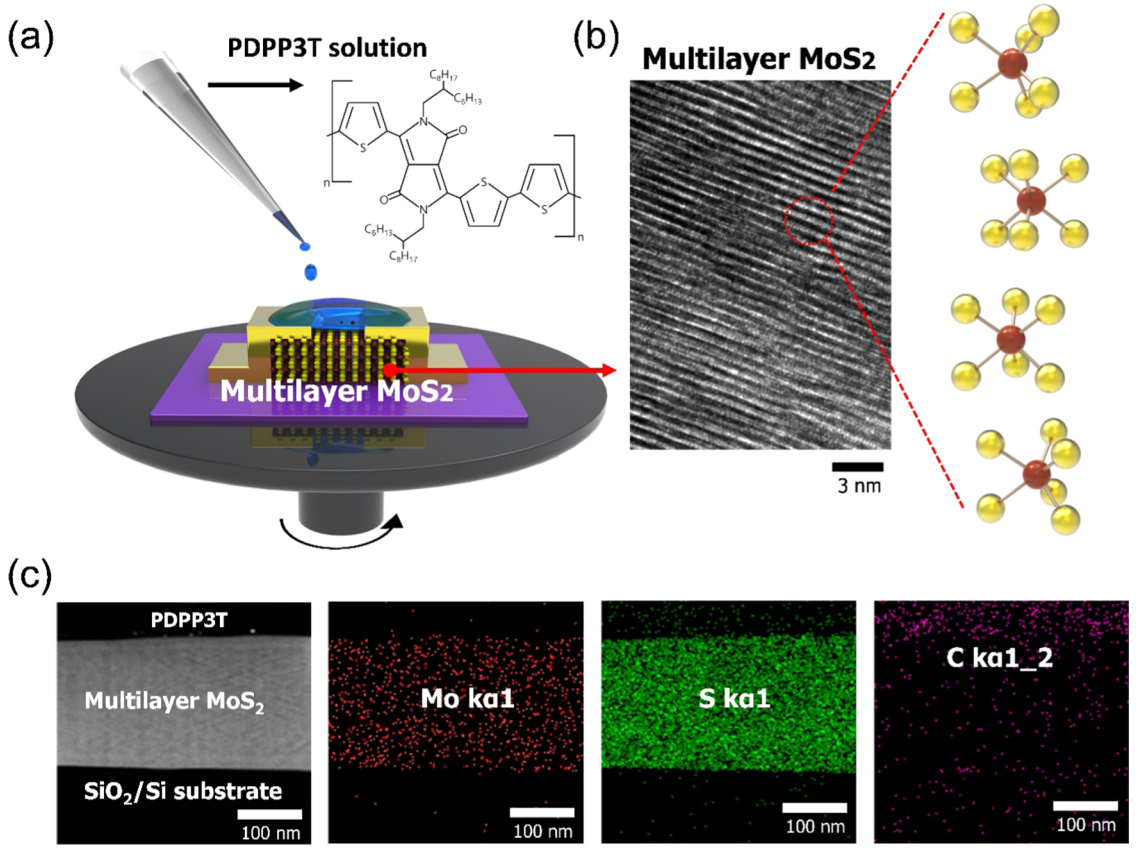

Figure 1. Fabrication of the HP-MoS_2. (a) Schematic process for the preparation of the HP-MoS_2. The inset is the molecular structure of PDPP3T (the doping material). (b) Cross-sectional TEM image of the multilayer MoS_2. The length of the scale bar is 4 nm (white). (c) Cross-sectional EDS mapping of the Mo (red dot), S (green dot), and C (magenta dot) distributions for the HP-MoS_2. The length of the scale bar is 100 nm (white).

TMDs offer great potential for these materials due to their simple fabrication.

Here, we present a chemical doping scheme for a multilayer MoS_2. We fabricated a heterogeneous poly-(diketopyrrolopyrrole-terthiophene) (PDPP3T)-multilayer MoS_2 (HP-MoS_2) transistor by simply coating poly-(diketopyrrolopyrrole-terthiophene) (PDPP3T) on a fabricated MoS_2 transistor. With an increase of annealing temperature (T_A), these manufactured devices exhibit a significant improvement in electrical properties, including transconductance and on-current properties. Using a comprehensive analysis of X-ray photoelectron spectroscopy (XPS) and grazing incidence wide-angle X-ray diffraction (GIWAXD), we also investigate the fundamental mechanisms that account for these electrical doping effects in multilayer MoS_2. We also demonstrate that TMD-based complementary metal−oxide−semiconductor (CMOS) inverter uses $MoSe_2$ and HP-MoS_2 as p- and n-channel semiconductors, respectively. The proposed CMOS inverter exhibits a full swing operation from V_{DD} to G_{ND} with sharp conversion.

EXPERIMENTAL SECTION

Device Fabrication. Mechanically exfoliated MoS_2 flakes from bulk MoS_2 (SPI crystals) were transferred onto a SiO_2/Si substrate. To form the source/drain electrodes on top of the MoS_2, a Ti (20 nm) and Au (100 nm) bilayer was deposited by E-beam evaporation. The electrical contacts were patterned using conventional photolithography and lift-off techniques. The devices were annealed at 200 °C for 2 h in a vacuum tube furnace under H_2 environment (100 sccm Ar and 10 sccm H_2) to remove residues. The channel width (W) and length (L) of the fabricated MoS_2 transistor were 1.62 and 4.11 μm, respectively. Then, PDPP3T (Solamer)[20] was dissolved in o-1,2-dichlorobenzene (ODCB) at a concentration of 7 mg mL^{-1} and dropped and spin-coated onto the as-fabricated multilayer MoS_2 transistor to complete the fabrication of the HP-MoS_2. The samples were annealed at T_A = 100, 200, and 300 °C in a nitrogen-purged glovebox.

Characterization. Two-dimensional (2D) GIWAXD experiments were conducted using the Pohang Light Source II (PLS-II) 9A beamline of the Pohang Accelerator Laboratory in Korea. Photon energy of 11.075 keV and an incidence angle of 0.15° were used with a 2D charge-coupled device detector (Rayonix, SX-165) to record the GIWAXD patterns. After Ar^+ ion sputtering at 2.5 keV to etch the PDPP3T surface, XPS measurements were performed at the Pohang Light Source II (PLS-II) 4D beamline of the Pohang Accelerator Laboratory in Korea. We performed Ar sputtering for 2 min to remove the PDPP3T upper layer, leaving the bottom MoS_2 unaffected. The applied power was 250 W with the target area of diameter ~1.5 cm at ultrahigh vacuum (=~10^{-6} torr). The electrical characteristics of the baseline MoS_2 and HP-MoS_2 transistors were measured using a parameter analyzer (Agilent 4156C instrument) at room temperature.

CMOS Inverter Fabrication. We used the $MoSe_2$ transistor and the HP-MoS_2 transistor as p-type and n-type channel, respectively, in the CMOS inverter. For the $MoSe_2$ transistor, we synthesized a $MoSe_2$ flake by the chemical vapor deposition (CVD) method. We placed molybdenum trioxide and Se powders in a quartz tube. Temperature used was ~800 °C in the vaporization and deposition zones of the quartz tube. The temperature was increased with a rate of 25 °C min^{-1}. Ar (120 sccm) and H_2 (20 sccm) flowed in the quartz tube during the entire process. We used high-pressure CVD growth method (>760 torr) to provide p-type-dominant semiconducting characteristics of the $MoSe_2$ transistor. After the synthesis of the

DOI: 10.1021/acsami.8b08773
ACS Appl. Mater. Interfaces XXXX, XXX, XXX−XXX

$MoSe_2$ flake, we deposited the source/drain electrodes (Ti, 20 nm and Au, 100 nm) using E-beam evaporation, which completed the fabrication of the $MoSe_2$ transistor. We externally connected the drain electrodes of the $MoSe_2$ transistor and the HP-MoS_2 transistor using probe station equipment and a switching box. The channel W and L of the n-type PDPP3T-MoS_2 transistor are 19.96 and 38.37 μm, respectively, and W and L of the p-type $MoSe_2$ transistor are 15.34 and 19.90 μm, respectively.

RESULTS AND DISCUSSION

Fabrication of the Heterogeneous PDPP3T-Multilayer MoS_2 Transistors. We first prepared multilayer MoS_2 transistors. By conventional lift-off lithography, source and drain electrode contacts (S/D) were deposited on top of the prepared multilayer MoS_2. We spin-coated the PDPP3T solution in an ODCB solution on top of the fabricated multilayer MoS_2 transistor. Figure 1a shows a schematic illustration of the fabrication process. To inspect the fabricated structure of the HP-MoS_2 transistors, we conducted cross-sectional transmission electron microscopy (TEM) and energy-dispersive X-ray spectroscopy (EDS) mapping. Figure 1b shows the measured TEM image, which shows the multilayer MoS_2 bulk. The EDS mappings (Figure 1c) also showed a uniform distribution of Mo and S in the MoS_2 layers as well as C in the PDPP3T coating. Further analysis (wide-scan of XPS) is provided in Figure S1, Supporting Information.

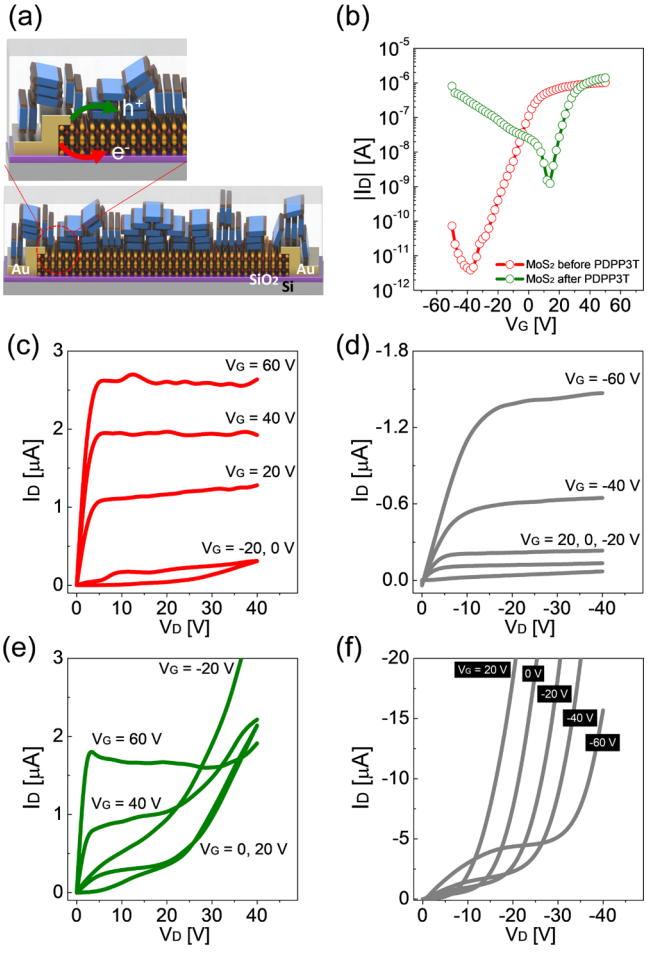

Figure 2. Device characteristics of the HP-MoS_2 transistors at T_A = 100 °C. (a) Schematic of the HP-MoS_2 transistors at T_A = 100 °C. PDPP3T has a coexisting edge-on and face-on molecular orientation. (b) Comparison of the transfer characteristics at V_D = 1 V. Red circle line: baseline MoS_2 transistor. Green circle line: HP-MoS_2 transistor. (c) Output curves of the baseline MoS_2 transistor. (d) Output curves of the pristine PDPP3T transistor. (e) Output curves of the HP-MoS_2 transistors at T_A = 100 °C. V_{GS} = −20, 0, 20, 40, 60 V. (f) Output curves of the HP-MoS_2 transistors at T_A = 100 °C. V_{GS} = 20, 0, −20, −40, −60 V.

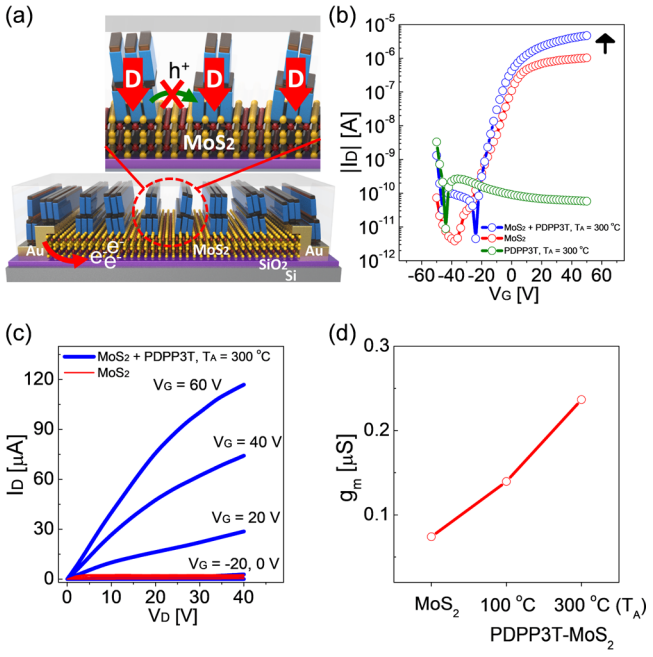

Figure 3. Device characteristics of the HP-MoS_2 transistors at T_A = 300 °C. (a) Schematic of the HP-MoS_2 transistors at T_A = 300 °C. PDPP3T has a strong edge-on orientation. (b) Comparison of the transfer characteristics at V_D = 1 V. Red circle line: baseline MoS_2 transistor. Green circle line: PDPP3T transistor at T_A = 300 °C. Blue circle line: HP-MoS_2 transistor at T_A = 300 °C. (c) Comparison of output curves. Red circle line: baseline MoS_2 transistor. Blue circle line: HP-MoS_2 transistor at T_A = 300 °C. (d) Comparison of the maximum transconductance (g_m) depending on the PDPP3T doping effect.

Electrical Characteristics of the Heterogeneous PDPP3T-Multilayer MoS_2 Transistors. We next investigated the electrical characteristics of the HP-MoS_2 transistors. To shed light on the doping effects, we measured the baseline multilayer MoS_2 transistor and then fabricated the HP-MoS_2 transistor using the same basic device. Therefore, the electrical characteristics were compared according to the presence of PDPP3T. Figure 2a shows a schematic of the manufactured HP-MoS_2 transistor structure. The electrical transfer characteristics (I_{DS}−V_{GS}) of the HP-MoS_2 transistor compared to the baseline MoS_2 transistor are shown in Figure 2b. The baseline MoS_2 transistor showed unipolar n-type operation (red circular line). In contrast, the HP-MoS_2 transistor exhibited an ambipolar behavior of coexisting p- and n-type currents (green circular line). As shown in Figure 2a, holes and electrons were injected into the upper PDPP3T and lower MoS_2, respectively, so that the HP-MoS_2 exhibited an ambipolar behavior. Figure 2c,d shows the output curves of the baseline MoS_2 transistor and pristine PDPP3T transistor, respectively. The measured output curves show that the baseline MoS_2 transistor provides unipolar n-type operation, whereas the pristine PDPP3T transistor provides unipolar p-type operation. Combination of MoS_2 and PDPP3T in the

DOI: 10.1021/acsami.8b08773
ACS Appl. Mater. Interfaces XXXX, XXX, XXX−XXX

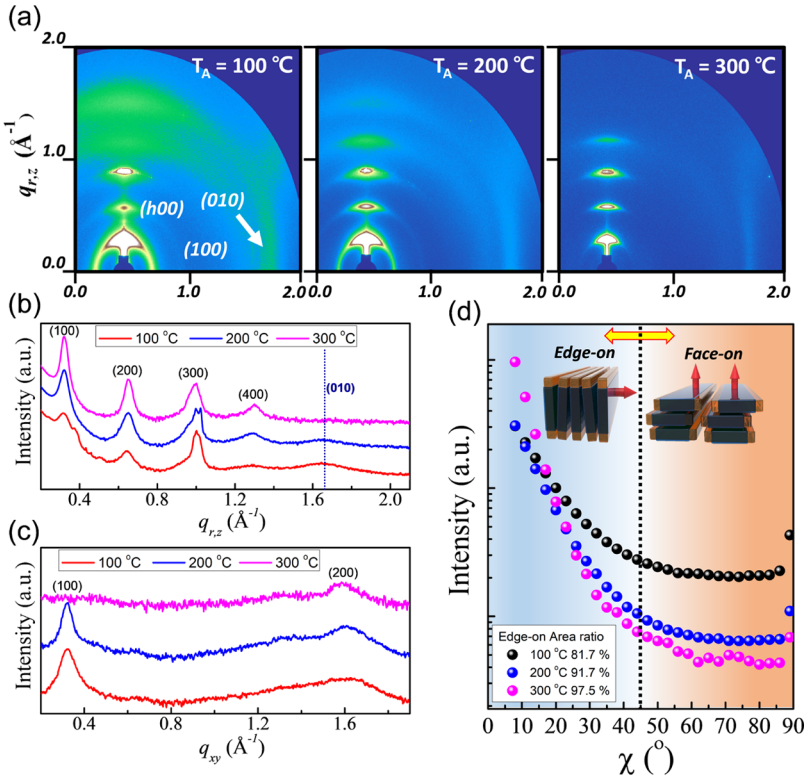

Figure 4. GIWAXD analysis of the HP-MoS_2. (a) GIWAXD images of the HP-MoS_2 at various T_A = 100, 200, and 300 °C. (b) Diffraction peak profiles along the out-of-plane direction. (c) Diffraction peak profiles along the in-plane direction. (d) Quantitative area ratio of the edge-on and face-on orientations.

channel of a transistor (i.e., the HP-MoS_2 transistor) showed both the hole and electron transport provided by MoS_2 and PDPP3T, respectively. These ambipolar characteristics of the HP-MoS_2 transistor are also shown in the output curves (Figure 2e,f). In the measured output curves, we observed that drain current (I_D) was not saturated over the whole range of V_D. This abnormal feature is attributed to the counter flow (hole in n-type operation/electron in p-type operation), which is typically observed in conventional ambipolar transistors.[21,22]

We also characterized the HP-MoS_2 transistor at a high annealing temperature (T_A = 300 °C) because the degree of T_A notably changes the molecular morphology of PDPP3T,[23] which can influence the electrical characteristics of the bottom multilayer MoS_2. Figure 3a shows a schematic of the HP-MoS_2 transistor annealed at 300 °C. Figure 3b shows the measured transfer characteristics of the HP-MoS_2 transistor at T_A = 300 °C with respect to that of the baseline MoS_2 transistor. Interestingly, at T_A = 300 °C, the HP-MoS_2 transistor no longer exhibited bipolar properties. Instead of exhibiting a current mixed with MoS_2 and PDPP3T, the device (blue circular line) provided the larger n-type current (~4.6×). This improvement resulted in a high current on/off ratio of 10^6 in the HP-MoS_2 transistor. The measured output curves also displayed an increase in the n-type current, as shown in Figure 3c. To evaluate the electrical doping effects of PDPP3T, we plotted the transconductance values (g_m) of the measured devices depending on the existence of PDPP3T and T_A (Figure 3d). The results suggest that the electron current was increased by PDPP3T doping. An analysis of the observed electrical enhancement (doping effect) by PDPP3T is provided in the next section.

Synchrotron-Based Analysis of the Heterogeneous PDPP3T-Multilayer MoS_2 Layers. To investigate the observed electrical doping effects of the HP-MoS_2 transistor, GIWAXD and XPS analyses were performed. We prepared HP-MoS_2 films at various T_A = 100, 200, and 300 °C to gain more insight into the doping effects depending on T_A. The details of the GIWAXD and XPS experiments are given in the Experimental Section. We first conducted GIWAXD analysis of the baseline MoS_2 film. The estimated crystal structure was equal to a = 3.163 and c = 12.295 Å. The observed (002) peak indicated that the MoS_2 crystal grew along the (002) plane.

Figure 4a–c shows the measured GIWAXD images of the HP-MoS_2 films at T_A = 100, 200, and 300 °C, respectively. In all of the measured GIWAXD images, diffraction peaks of PDPP3T were observed. A notable difference between the measured GIWAXD results of the samples at various T_A values is the molecular orientation of the PDPP3T. At T_A = 100 °C, coexisting edge-on and face-on orientation peaks were observed out-of-plane and in-plane, respectively. In contrast, the sample at a higher T_A = 200 °C showed an increased intensity of diffraction peaks along the out-of-plane direction, indicating that a larger molecular orientation occurred in the edge-on orientation. A more significant change in the measured GIWAXD result was observed in the sample at T_A = 300 °C. The (h00) reflections along the out-of-plane direction became stronger, which indicates that the edge-on crystallites were improved. On the other hand, the (010) reflection along the in-plane direction disappeared, indicating that the crystallinity of the film for the face-on orientation became weak at high-temperature annealing of T_A = 300 °C. To gain more insight into the observed changes in the PDPP3T molecular orientation, we quantitatively compared

DOI: 10.1021/acsami.8b08773
ACS Appl. Mater. Interfaces XXXX, XXX, XXX−XXX

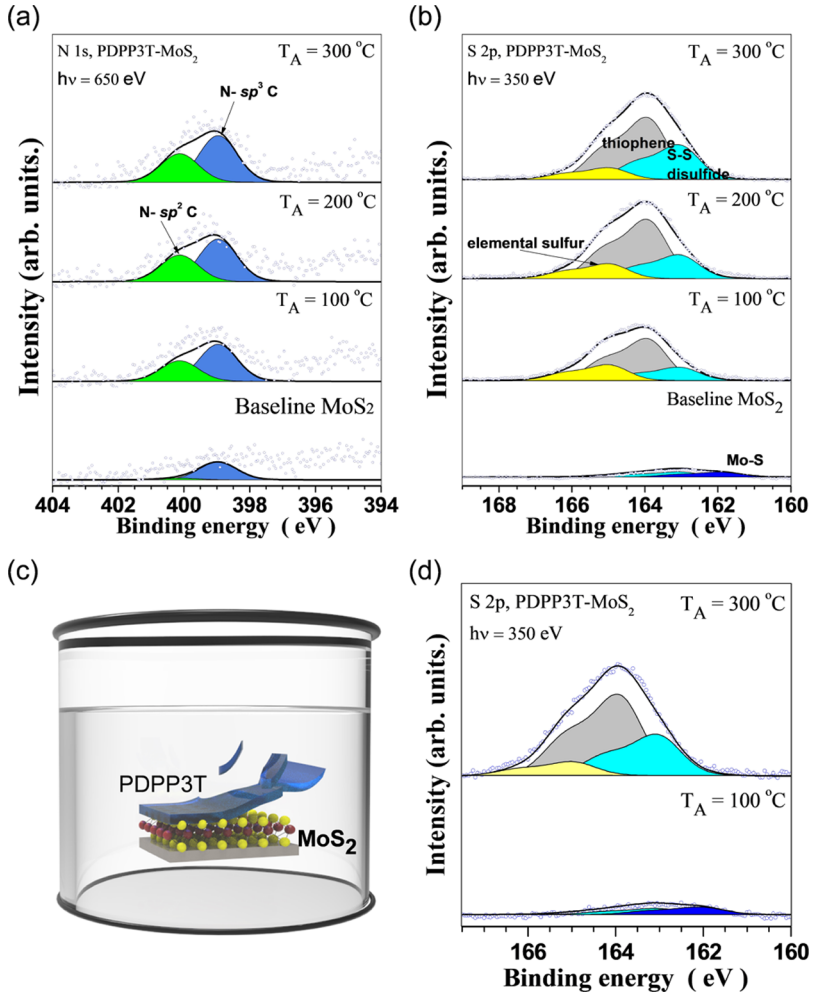

Figure 5. XPS analysis of the HP-MoS_2. (a) N 1s core level spectra of the HP-MoS_2 at various T_A = 100, 200, and 300 °C. (b) S 2s core level spectra of the HP-MoS_2 at various T_A = 100, 200, and 300 °C. (c) Schematic illustration showing the XPS measurement after dipping the samples in chloroform solvent. (d) S 2s core level spectra of the HP-MoS_2 at various T_A = 100 and 300 °C after dipping the samples in chloroform solvent.

the percentage of edge-on and face-on distributions by azimuth scan analysis (Figure 4d). Nearly perfect edge-on crystallites (97.5%) appeared at T_A = 300 °C, but lower edge-on crystallinity (81.7 and 91.7%) was observed at T_A = 100 and 200 °C. On the basis of these investigations, we concluded that high-temperature annealing can change PDPP3T films to a strong edge-on molecular orientation.

To provide further analysis of the PDPP3T doping effects, XPS was performed. We prepared HP-MoS_2 films at various T_A = 100, 200, and 300 °C to observe the chemical composition changes. We obtained N 1s and S 2p spectra of the prepared samples after removing the top PDPP3T by argon (Ar) sputtering, which allowed us to investigate the interface between the PDPP3T and MoS_2 layers. Figure 5a,b shows the measured N 1s and S 2p spectra, respectively. The observed sp^2 C−N, sp^3 C−N, and thiophene (~164 eV) indicate the existence of PDPP3T.[23] A notable change in the measured spectra at various T_A values occurs for the intensities of N 1s and S 2p. With the increase of T_A, the intensities of N 1s and S 2p became larger, which indicates that the N and S concentrations (parts of the PDPP3T) were gradually increased. To gain further insight into the observed change of the chemical composition, we measured the N 1s and S 2p spectra again after dipping the samples at T_A = 100 and 300 °C in chloroform (CF) for 12 h (Figure 5c). For the sample at T_A = 100 °C, the previously measured N 1s and S 2p spectra disappeared, indicating that PDPP3T was fully removed by dipping in CF (Figure 5d). In contrast, for the sample at T_A = 300 °C, the previously measured N 1s and S 2p spectra were maintained after dipping in CF (Figure 5d). This result indicates that PDPP3T still existed on the MoS_2 layer despite dipping in CF. The two experiments suggest that the interaction between PDPP3T and the MoS_2 layer became larger at high-temperature annealing of T_A = 300 °C and hence PDPP3T remained unremoved even after both argon (Ar) sputtering and dipping in CF.

On the basis of the synchrotron-based analyses of GIWAXD and XPS, we emphasize the two measured observations: (1) edge-on crystallites of PDPP3T and (2) larger interaction between PDPP3T and MoS_2 at high-temperature annealing. We first observed that PDPP3T exhibited strong edge-on crystallites (97.5%) at T_A = 300 °C. As the molecular orientation of PDPP3T is changed from random to a strong edge-on domain, a stronger dipole moment occurs. Since the total molecular dipole moment is equal to the sum of each component molecule dipole, the aligned PDPP3T at T_A = 300 °C can induce a larger dipole moment on the bottom MoS_2 layer. Furthermore, the larger interaction between the PDPP3T and MoS_2 indicates that the distance between the two materials became closer. As the distance is decreased, not

DOI: 10.1021/acsami.8b08773
ACS Appl. Mater. Interfaces XXXX, XXX, XXX−XXX

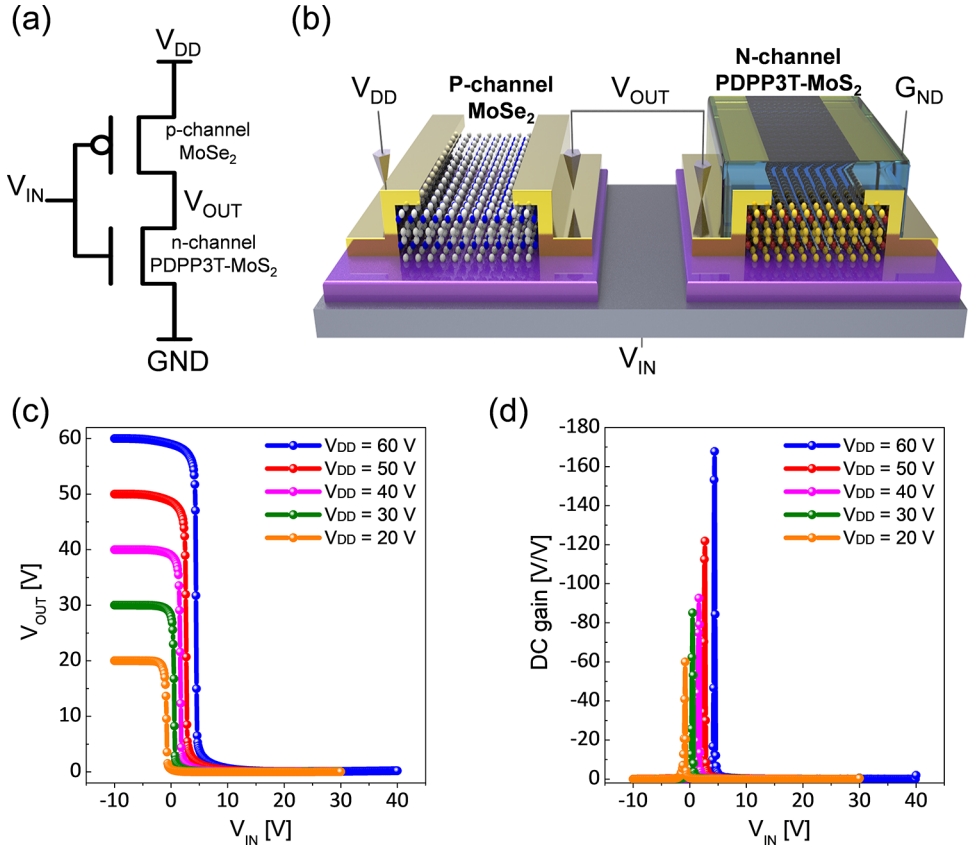

Figure 6. CMOS inverter. (a) Schematic symbol and (b) schematic structure of CMOS inverter circuit based on p-type $MoSe_2$ and n-type PDPP3T-MoS_2 transistors. (c) Voltage transfer characteristics at various V_{DD}. (d) Corresponding DC gain values.

only is a higher dipole induced but also a charge transfer doping can occur. PDPP3T comprises three thiophenes, where there is a lone pair of electrons located at the sulfur. These lone pairs are expected to result in negative charge transfer to the MoS_2 layer. The aforementioned electrical enhancement at T_A = 300 °C supports the dipole and charge transfer effects. The induced dipole effect reduces the SB height and thus leads to the creation of excess carriers (Δn). The negative charge transfer from thiophene to MoS_2 can also provide Δn.

To provide further analysis, we investigated the contact resistance (R_P) and carrier concentration (N) depending on the PDPP3T doping effect. Using transfer line method, we extracted R_C. In the baseline MoS_2 transistor (Figure S2, Supporting Information), a large R_C was observed ($2R_C$ = 1.18 × 10^7 Ω cm at V_D = 5 V and $2R_C$ = 5.98 × 10^6 Ω cm at V_D = 10 V). After PDPP3T doping, the transistor exhibited a significant improvement ($2R_C$ = 4.48 × 10^5 Ω cm at V_D = 5 V and $2R_C$ = 2.7 × 10^5 Ω cm at V_D = 10 V) in contact resistance. We extracted N of the transistors by measuring the capacitance−voltage (C−V) characteristic curves of MoS_2 devices before/after PDPP3T doping (Figure S3, Supporting Information). The N of the baseline MoS_2 transistor was estimated to be 2.3 × 10^{15} cm^{-3}, which is well agreed with the previous report. After PDPP3T doping, N increased by ∼6 times (N = 1.4 × 10^{16} cm^{-3}) than that of the baseline transistor. Therefore, the reduced R_P and the increased N account for the enhancement of I_D.

CMOS Inverter. Using the proposed HP-MoS_2 transistor, we next demonstrated a CMOS inverter that uses $MoSe_2$ PMOS and HP-MoS_2 NMOS. The fabricated inverter comprises a $MoSe_2$ transistor and HP-MoS_2 transistor at T_A = 300 °C as the p- and n-channel, respectively. Figure 6a,b shows a schematic symbol and the structure of the manufactured inverter. The inverter was fabricated by externally connecting two transistors on different substrates. The electrical characteristics of the p-type $MoSe_2$ transistor and the n-type PDPP3T-MoS_2 transistor are shown in Figure S4. Further details of the CMOS inverter are given in the Experimental Section. Figure 6c shows the static voltage transfer characteristics (V_{in}−V_{out} curve) of the fabricated CMOS inverter at various V_{DD} = 20−60 V. The measured V_{in}−V_{out} curves exhibited a logic inversion with an output swing of ∼100%. We plotted the measured voltage gain profile with respect to V_{in}, which resulted in direct current (DC) gain = 60−170 V/V depending on the applied V_{DD}.

CONCLUSIONS

In summary, we developed a high-performance multilayer MoS_2 transistor by means of doping effects of PDPP3T. The fabricated HP-MoS_2 transistor enhanced the n-type current at T_A = 300 °C. We performed fundamental analyses of this enhancement by GIWAXD and XPS. We also developed the CMOS inverter that uses the n-type HP-MoS_2 and the p-type $MoSe_2$ transistors, which exhibited a full swing from V_{DD} to G_{ND} as a function of V_{in}. On the basis of our proposed doping scheme and devices as well as the analyses, we believe that this result is a step toward developing next-generation semiconductor devices in the emerging field of applications.

DOI: 10.1021/acsami.8b08773
ACS Appl. Mater. Interfaces XXXX, XXX, XXX−XXX

■ ASSOCIATED CONTENT

Supporting Information

The Supporting Information is available free of charge on the ACS Publications website at DOI: 10.1021/acsami.8b08773.

Wide-scan XPS spectra (Figure S1); optical microscopy image, measured total resistance for contact resistance extraction (Figure S2); schematic illustration of the capacitance−voltage ($C-V$) measurement, comparison of the $C-V$ characteristic curves for the extraction of the carrier concentration (N) (Figure S3); I_D-V_G transfer characteristics (Figure S4) (PDF)

■ AUTHOR INFORMATION

Corresponding Authors

*E-mail: kimskcnt@gmail.com (S.K.).
*E-mail: jaejoon@postech.ac.kr (J.-J.K.).

ORCID

Sunkook Kim: 0000-0003-1747-4539

Author Contributions

H.Y. and S.H. contributed equally to this work.

Notes

The authors declare no competing financial interest.

■ ACKNOWLEDGMENTS

This work was supported by Ministry of Trade, Industry, and Energy (MOTIE) and Korea Evaluation Industrial Technology (KEIT) through the Industrial Strategic Technology Development Program (Nos. 10079571 and 1004515) and by the National Research Foundation of Korea (NRF) grant (No. NRF-2015R1A1A1A05027488). This research was also supported in part by the Ministry of Science, ICT and Future Planning (MSIP), Korea, under the "ICT Consilience Creative Program" (IITP-2018-2011-1-00783) supervised by the Institute for Information & Communications Technology Promotion (IITP), by the National Research Foundation of Korea (NRF) grant funded by the Korea government (MSIP) (No. NRF-2017R1A2B4006749 and 2018R1A2B2003558).

■ REFERENCES

(1) Jariwala, D.; Sangwan, V. K.; Late, D. J.; Johns, J. E.; Dravid, V. P.; Marks, T. J.; Lauhon, L. J.; Hersam, M. C. Band-like Transport in High Mobility Unencapsulated Single-Layer MoS2 Transistors. *Appl. Phys. Lett.* **2013**, *102*, No. 173107.

(2) Kappera, R.; Voiry, D.; Yalcin, S. E.; Branch, B.; Gupta, G.; Mohite, A. D.; Chhowalla, M. Phase-Engineered Low-Resistance Contacts for Ultrathin MoS2 Transistors. *Nat. Mater.* **2014**, *13*, 1128−1134.

(3) Shi, Y.; Li, H.; Li, L.-J. Recent Advances in Controlled Synthesis of Two-Dimensional Transition Metal Dichalcogenides via Vapour Deposition Techniques. *Chem. Soc. Rev.* **2015**, *44*, 2744−2756.

(4) Wang, Q. H.; Kalantar-Zadeh, K.; Kis, A.; Coleman, J. N.; Strano, M. S. Electronics and Optoelectronics of Two-Dimensional Transition Metal Dichalcogenides. *Nat. Nanotechnol.* **2012**, *7*, 699−712.

(5) Wang, H.; Yu, L.; Lee, Y.-H.; Shi, Y.; Hsu, A.; Chin, M. L.; Li, L.-J.; Dubey, M.; Kong, J.; Palacios, T. Integrated Circuits Based on Bilayer MoS2 Transistors. *Nano Lett.* **2012**, *12*, 4674−4680.

(6) Cheng, R.; Jiang, S.; Chen, Y.; Liu, Y.; Weiss, N.; Cheng, H.-C.; Wu, H.; Huang, Y.; Duan, X. Few-Layer Molybdenum Disulfide Transistors and Circuits for High-Speed Flexible Electronics. *Nat. Commun.* **2014**, *5*, No. 5143.

(7) Hang, Y.; Li, Q.; Luo, W.; He, Y.; Zhang, X.; Peng, G. Photo-Electrical Properties of Trilayer MoSe2 Nanoflakes. *Nano* **2016**, *11*, No. 1650082.

(8) Nam, H.; Oh, B.-R.; Chen, P.; Chen, M.; Wi, S.; Wan, W.; Kurabayashi, K.; Liang, X. Multiple MoS2 Transistors for Sensing Molecule Interaction Kinetics. *Sci. Rep.* **2015**, *5*, No. 10546.

(9) Zhang, Y.; Ye, J.; Matsuhashi, Y.; Iwasa, Y. Ambipolar MoS2 Thin Flake Transistors. *Nano Lett.* **2012**, *12*, 1136−1140.

(10) Mann, J.; Ma, Q.; Odenthal, P. M.; Isarraraz, M.; Le, D.; Preciado, E.; Barroso, D.; Yamaguchi, K.; Von Son Palacio, G.; Nguyen, A.; Tran, T.; Wurch, M.; Nguyen, A.; Klee, V.; Bobek, S.; Sun, D.; Heinz, T. F.; Rahman, T. S.; Kawakami, R.; Bartels, L. 2-Dimensional Transition Metal Dichalcogenides with Tunable Direct Band Gaps: MoS2(1-x)Se2x Monolayers. *Adv. Mater.* **2014**, *26*, 1399−1404.

(11) Zhu, W.; Yogeesh, M. N.; Yang, S.; Aldave, S. H.; Kim, J. S.; Sonde, S.; Tao, L.; Lu, N.; Akinwande, D. Flexible Black Phosphorus Ambipolar Transistors, Circuits and AM Demodulator. *Nano Lett.* **2015**, *15*, 1883−1890.

(12) Kim, S.; Konar, A.; Hwang, W.-S.; Lee, J. H.; Lee, J.; Yang, J.; Jung, C.; Kim, H.; Yoo, J.-B.; Choi, J.-Y.; Jin, Y. W.; Lee, S. Y.; Jena, D.; Choi, W.; Kim, K. High-Mobility and Low-Power Thin-Film Transistors Based on Multilayer MoS2 Crystals. *Nat. Commun.* **2012**, *3*, No. 1011.

(13) Jung, C.; Kim, S. M.; Moon, H.; Han, G.; Kwon, J.; Hong, Y. K.; Omkaram, I.; Yoon, Y.; Kim, S.; Park, J. Highly Crystalline CVD-Grown Multilayer MoSe2 Thin Film Transistor for Fast Photo-detector. *Sci. Rep.* **2015**, *5*, No. 15313.

(14) Song, W. G.; Kwon, H.; Park, J.; Yeo, J.; Kim, M.; Park, S.; Yun, S.; Kyung, K.; Grigoropoulos, C. P.; Kim, S.; Hong, Y. K. High Performance Flexible Multilayer MoS2 Transistors on Solution Based Polyimide Substrates. *Adv. Funct. Mater.* **2016**, *26*, 2426−2434.

(15) Choi, W.; Cho, M. Y.; Konar, A.; Lee, J. H.; Cha, G. B.; Hong, S. C.; Kim, S.; Kim, J.; Jena, D.; Joo, J.; Kim, S. High-Detectivity Multilayer MoS2 Phototransistors with Spectral Response from Ultraviolet to Infrared. *Adv. Mater.* **2012**, *24*, 5832−5836.

(16) Kiriya, D.; Tosun, M.; Zhao, P.; Kang, J. S.; Javey, A. Air-Stable Surface Charge Transfer Doping of MoS_2 by Benzyl Viologen. *J. Am. Chem. Soc.* **2014**, *136*, 7853−7856.

(17) Yu, L.; Zubair, A.; Santos, E. J. G.; Zhang, X.; Lin, Y.; Zhang, Y.; Palacios, T. High-Performance WSe2 Complementary Metal Oxide Semiconductor Technology and Integrated Circuits. *Nano Lett.* **2015**, *15*, 4928−4934.

(18) Kang, D.-H.; Shim, J.; Jang, S. K.; Jeon, J.; Jeon, M. H.; Yeom, G. Y.; Jung, W. S.; Jang, Y. H.; Lee, S.; Park, J.-H. Controllable Nondegenerate P-Type Doping of Tungsten Diselenide by Octadecyltrichlorosilane. *ACS Nano* **2015**, *9*, 1099−1107.

(19) Park, H.-Y.; Lim, M.-H.; Jeon, J.; Yoo, G.; Kang, D.-H.; Jang, S. K.; Jeon, M. H.; Lee, Y.; Cho, J. H.; Yeom, G. Y.; Jung, W. S.; Lee, J.; Park, S.; Lee, S.; Park, J.-H. Wide-Range Controllable n-Doping of Molybdenum Disulfide (MoS2) through Thermal and Optical Activation. *ACS Nano* **2015**, *9*, 2368−2376.

(20) Yoo, H.; Ghittorelli, M.; Smits, E. C. P.; Gelinck, G. H.; Lee, H.; Torricelli, F.; Kim, J. Reconfigurable Complementary Logic Circuits with Ambipolar Organic Transistors. *Sci. Rep.* **2016**, *6*, No. 35585.

(21) Anthopoulos, T. D.; Setayesh, S.; Smits, E.; Cölle, M.; Cantatore, E.; De Boer, B.; Blom, P. W. M.; De Leeuw, D. M. Air-Stable Complementary-like Circuits Based on Organic Ambipolar Transistors. *Adv. Mater.* **2006**, *18*, 1900−1904.

(22) Zhu, W.; Yogeesh, M. N.; Yang, S.; Aldave, S. H.; Kim, J. S.; Sonde, S.; Tao, L.; Lu, N.; Akinwande, D. Flexible Black Phosphorus Ambipolar Transistors, Circuits and AM Demodulator. *Nano Lett.* **2015**, *15*, 1883−1890.

(23) Yoo, H.; Ghittorelli, M.; Lee, D.-K.; Smits, E. C. P.; Gelinck, G. H.; Ahn, H.; Lee, H.-K.; Torricelli, F.; Kim, J.-J. Balancing Hole and Electron Conduction in Ambipolar Split-Gate Thin-Film Transistors. *Sci. Rep.* **2017**, *7*, No. 5015.

DOI: 10.1021/acsami.8b08773
ACS Appl. Mater. Interfaces XXXX, XXX, XXX−XXX